Available online at www.sciencedirect.com
SCIENCE DIRECT®
Journal of Solid State Chemistry 177 (2004) 1867–1872
JOURNAL OF SOLID STATE CHEMISTRY
http://elsevier.com/locate/jssc

Crystal structures of $CsFe_2S_3$ and $RbFe_2S_3$: synthetic analogs of rasvumite KFe_2S_3

Roger H. Mitchell,* Kirk C. Ross, and Eric G. Potter

Department of Geology, Lakehead University, 955 Oliver Road, Thunder Bay, Ontario, Canada P7B 5E1

Received 7 November 2003; received in revised form 30 December 2003; accepted 14 January 2004

Abstract

The isostructural alkali thioferrate compounds $CsFe_2S_3$, $RbFe_2S_3$ and KFe_2S_3 have been synthesized by reacting Fe and S with their corresponding $AFeS_2$ (A = K, Rb, Cs) precursors. The crystal structures of these and binary compounds of intermediate composition were determined by Rietveld analysis of laboratory powder X-ray diffraction patterns. All of the synthesized compounds adopt the space group *Cmcm* (#63), $Z = 4$ with: $a = 9.5193(8)$ Å, $b = 11.5826(10)$ Å, $c = 5.4820(4)$ Å for $CsFe_2S_3$; $a = 9.2202(7)$ Å, $b = 11.2429(9)$ Å, $c = 5.4450(3)$ Å for $RbFe_2S_3$; and $a = 9.0415(13)$ Å, $b = 11.0298(17)$ Å, $c = 5.4177(6)$ Å for KFe_2S_3. These mixed valence alkali thioferrates show regular changes in cell dimensions, AS_{10} (A = K, Rb, Cs) polyhedron volumes, polyhedron distortion parameters, and calculated oxidation state of Fe with respect to increasing size of the alkali element cation. The calculated empirical oxidation state of iron varies from +2.618 ($CsFe_2S_3$), through +2.666 ($RbFe_2S_3$) to +2.77 (KFe_2S_3).
© 2004 Elsevier Inc. All rights reserved.

Keywords: Rasvumite; Alkali thioferrate; Crystal structure; Rietveld refinement

1. Introduction

Rasvumite, KFe_2S_3, is a naturally occurring mixed valence alkali thioferrate characterized by the presence of edge-sharing double chains of FeS_4 polyhedra [1]. The material is of interest to solid state chemists because of the intermediate oxidation state of the transition metal, and to geochemists as the mineral is one of the few terrestrial examples of potassium exhibiting chalcophile behavior in a relatively oxidizing environment [2]. Recently, Chakhmouradian et al. [3] reported the presence of Rb- and Cs-bearing rasvumite (6.5–7.4 wt% Rb; 1.6–2.9 wt% Cs) in peralkaline syenitic rocks occurring at Mt. Saint-Hilaire, Quebec. This discovery suggested that the Rb- and Cs analogues of rasvumite, $RbFe_2S_3$ and $CsFe_2S_3$, should exist. Surprisingly, these compounds do not appear to have been synthesized, although the corresponding ternary iron chalcogenides AFe_2X_3 (A = Rb, Cs; X = Se, Te) have been prepared by Klepp et al. [4]. Accordingly, this paper describes the preparation and structure determination of $RbFe_2S_3$ and $CsFe_2S_3$ and compounds of intermediate composition between these end-members and KFe_2S_3.

2. Experimental

Starting materials for the synthesis of all compounds were: iron; sulfur; Rb_2CO_3; Cs_2CO_3; K_2CO_3 (all 99.999% Aldrich Chemical Co.). The syntheses were achieved using a two step reaction using the corresponding intermediate alkali thioferrate compounds ($AFeS_2$; A = K, Rb, Cs) as precursors. The thioferrates were prepared following the procedure outlined by Brauer [5]. The formation of these intermediate compounds involved combining iron powder obtained by reduction with H_2, sulfur and alkali carbonates in an agate mortar. The powder was loaded into a quartz boat, placed in a horizontal tube furnace under flowing nitrogen and heated at a rate of 15°C/min to 950°C. The sample was held at this temperature for 50 min, then cooled at a rate of 10°C/min to room temperature. The resultant material was washed and decanted with warm water, until only needles of thioferrate remained.

*Corresponding author. Fax: +807-346-7853.
E-mail address: roger.mitchell@lakeheadu.ca, rmitchel@lakeheadu.ca (R.H. Mitchell).

0022-4596/$ - see front matter © 2004 Elsevier Inc. All rights reserved.
doi:10.1016/j.jssc.2004.01.007

Table 1
Cell parameters for $CsFe_2S_3$, $RbFe_2S_3$, KFe_2S_3 and intermediate solid solution members

	$CsFe_2S_3$	$Cs_{0.5}Rb_{0.5}Fe_2S_3$	$RbFe_2S_3$	$Rb_{0.5}K_{0.5}Fe_2S_3$	KFe_2S_3	$K_{0.5}Cs_{0.5}Fe_2S_3$
a (Å)	9.5193(8)	9.4144(7)	9.2202(7)	9.1554(9)	9.0415(13)	9.3268(10)
b (Å)	11.5826(10)	11.4632(9)	11.2429(9)	11.1612(11)	11.0298(17)	11.3693(12)
c (Å)	5.4820(4)	5.4691(3)	5.4450(3)	5.4382(4)	5.41771(6)	5.4592(5)
V (Å)	604.438	590.223	564.436	555.711	540.286	578.891
R_{bragg}	2.96	3.69	3.83	3.43	5.43	3.61
R_{wp}	15.05	10.31	13.35	14.37	15.73	12.21
R_{exp}	12.97	7.39	10.65	11.83	8.42	7.60
GOF	1.16	1.40	1.25	1.22	1.87	1.61
D–W	1.56	1.08	1.32	1.45	0.59	0.87

GOF = goodness-of-fit; D–W = Durbin–Watson parameter.

Reduced iron and sulfur were subsequently mixed with the thioferrates in stoichiometric proportions. After drying at 110°C, the mixture was loaded into an evacuated quartz tube, which was inserted into a horizontal tube furnace at 500°C for 24 h and quickly air-quenched upon removal. The reactions occurring are summarized below:

$$6Fe + 4A_2CO_3 + 13S = 6AFeS_2 + A_2SO_4 + 4CO_2, \quad (1)$$

$$AFeS_2 + Fe + S = AFe_2S_3, \quad (2)$$

where A = K, Rb or Cs.

Using these experimental conditions it was found possible to form $RbFe_2S_3$ and $CsFe_2S_3$ containing only minor amounts of newly formed contaminants or relict thioferrate precursors. In contrast relatively pure KFe_2S_3 could not be prepared as diverse iron sulfides were typically also formed (see below). Binary solid solutions were prepared by similar methods.

Synthesized materials were examined at room temperature by powder X-ray diffraction (XRD) immediately after their preparation because of their instability in air. Data were collected using a Phillips P3710 diffractometer with a graphite monochromator and APD powder diffraction software. XRD step scans were collected using a 0.02° step for 4 s over a range of 18–100° for 2θ with monochromatic Cu$K\alpha$ radiation. The XRD patterns were inspected using the Bruker AXS software package EVA to identify the phases present and confirm that rasvumite-structured compounds were present. Data were further analyzed by Rietveld methods using the Bruker AXS software package TOPAS Version 2.1 operated in the fundamental parameters mode [6]. This recently introduced Windows-based software provides significant improvements in the ease of undertaking Rietveld refinements over commonly used DOS-based software such as FULLPROF [7]. Results obtained by either of these programs are similar. For example the cell dimensions and positional parameters of $RbFe_2S_3$ refined using TOPAS 2.1 with fundamental parameters and by FULLPROF with a Pseudo-Voigt peak shape function are in agreement within experimental errors (Table 2).

Depending upon the presence of impurities the number of TOPAS 2.1 refined variables ranged from 46 to 67 independent parameters. These included: zero corrections; scaling factors; Lorenz polarization corrections; cell dimensions; atomic positional coordinates; preferred orientation corrections; crystal size and strain effects; and isotopic thermal parameters. All refinements used as starting values the cell dimensions and atomic positional coordinates of rasvumite as given by Clark and Brown [1], and were refined assuming that all of the synthetic compounds crystallized in the space group *Cmcm* (#63) with the rasvumite structure [1]. Crystal structure data incorporated into the refinements for relict *C*2/*c* $KFeS_2$, *C*2/*c* $RbFeS_2$ and *Immm* $CsFeS_2$, were taken from Bronger et al. [8] and Bronger [9], and for $P6_3mc$ hexagonal $Fe_{1-x}S$ from Fasiska [10]. Up to 5 minor peaks arising from unidentified impurities were modelled and included in the background of the refinement as full profile peaks. Table 1 gives final Rietveld fitting parameters for the six rasvumite-structured compounds synthesized. Acceptable refinements were possible for all compounds, with the poorest agreement factors and R-values being for KFe_2S_3 which contained the most impurity phases (see below). The Rietveld refinements indicated that the amounts (wt%) of the desired compound and the impurities present in the synthesized materials were as follows: (1) $CsFe_2S_3$ (92.14), $CsFeS_2$ (7.86); (2) $RbFe_2S_3$ (90.03); $RbFeS_2$ (7.34); $Fe_{1-x}S$ (2.63); (3) KFe_2S_3 (52.77), $KFeS_2$ (44.11); $Fe_{1-x}S$ (3.12). Despite numerous attempts using different synthesis conditions we were unable to improve the yield of KFe_2S_3. Fig. 1 illustrates the powder X-ray diffraction pattern and Rietveld refinement difference plot of $CsFe_2S_3$.

3. Crystal structures

Tables 1 and 2 give refined cell dimensions, positional and isotropic thermal parameters for $CsFe_2S_3$, $RbFe_2S_3$

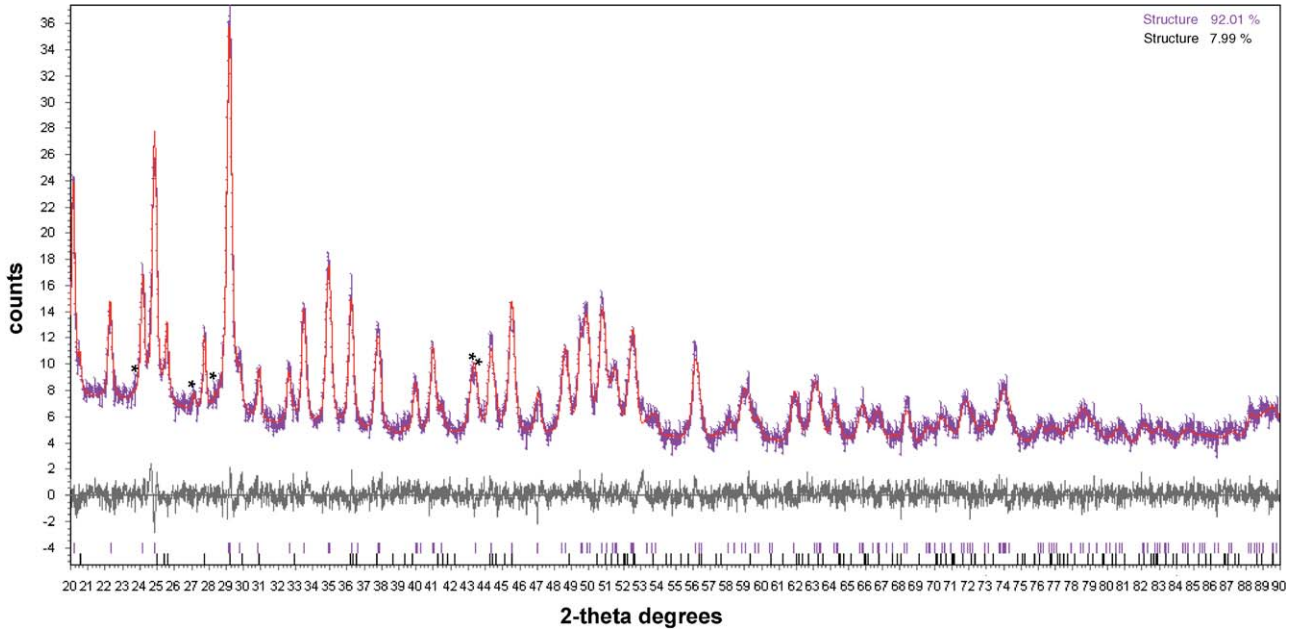

Fig. 1. Powder X-ray diffraction pattern of $CsFe_2S_3$ and Rietveld refinement difference plot. Upper and lower series of tick marks indicated calculated positions of reflections for $CsFe_2S_3$ and $CsFeS_2$, respectively. Asterisks indicate unidentified minor impurity phase. Count intensity is arbitrary and reflects scaling factors used in the Rietveld refinement.

Table 2
Positional and thermal parameters for $CsFe_2S_3$, $RbFe_2S_3$ and KFe_2S_3

	x	*y*	*z*	*B*
$CsFe_2S_3$				
Cs	0.5	0.1684(3)	0.25	1.44(15)
Fe	0.3582(5)	0.5	0	0.51(12)
S(1)	0.5	0.6155(9)	0.25	1.50(18)
S(2)	0.2302(8)	0.3932(7)	0.25	1.50(18)
$RbFe_2S_3$				
Rb	0.5	0.1687(3)	0.25	1.40(14)
		0.1687(4)		*1.78(15)*
Fe	0.3527(4)	0.5	0	0.50(13)
	0.3523(4)			*0.96(10)*
S(1)	0.5	0.6178(8)	0.25	1.50(14)
		0.6151(7)		*1.24(10)*
S(2)	0.2235(6)	0.3874(5)	0.25	1.50(14)
	0.2256(6)	*0.3902(5)*		*1.24(10)*
KFe_2S_3				
K	0.5	0.1744(13)	0.25	1.58(14)
Fe	0.3488(9)	0.5	0	0.39(13)
S(1)	0.5	0.6159(15)	0.25	0.62(15)
S(2)	0.2155(12)	0.3852(11)	0.25	0.62(15)

For $RbFe_2S_3$ data in italics are for a Rietveld refinement using FULLPROF [7] with $R_{bragg} = 5.38\%$.

Table 3
Positional and thermal parameters for AFe_2S_3 rasvumites (A = Cs, Rb, K)

	x	*y*	*z*	*B*
$(Cs_{0.5}Rb_{0.5})Fe_2S_3$				
Cs, Rb	0.5	0.1674(2)	0.25	1.11(14)
Fe	0.3563(3)	0.5	0	1.63(13)
S(1)	0.5	0.6190(6)	0.25	1.40(14)
S(2)	0.2234(5)	0.3892(4)	0.25	1.40(14)
$(Rb_{0.5}K_{0.5})Fe_2S_3$				
Rb, K	0.5	0.1694(4)	0.25	1.40(13)
Fe	0.3519(4)	0.5	0	0.50(11)
S(1)	0.5	0.6148(8)	0.25	1.50(13)
S(2)	0.2210(6)	0.3870(5)	0.25	1.50(13)
$(Cs_{0.5}K_{0.5})Fe_2S_3$				
Cs, K	0.5	0.1676(3)	0.25	1.40(14)
Fe	0.3513(4)	0.5	0	1.00(12)
S(1)	0.5	0.6187(9)	0.25	2.50(13)
S(2)	0.2252(7)	0.3863(6)	0.25	2.50(13)

and KFe_2S_3. Tables 1 and 3 give these data for some compositions intermediate between these end-members. All compounds crystallize in space group *Cmcm* (#63) and adopt the rasvumite structure. This consists of chains of double edge-sharing Fe–S tetrahedra aligned along the *c*-axis (Fig. 2). Alkali elements occupy the interstices between these chains and can be considered to form double chains of face-sharing pairs of 10-fold coordinated *A*–S polyhedra (A = K, Rb, Cs) also aligned along *c*. Regardless of the poor synthesis yield, the cell dimensions and positional coordinates determined for KFe_2S_3 in this work are in good agreement with those determined previously by Clark and Brown [1], i.e., $a = 9.049(6)$, $b = 11.019(7)$, $c = 5.431(4)$ Å, using single crystal methods.

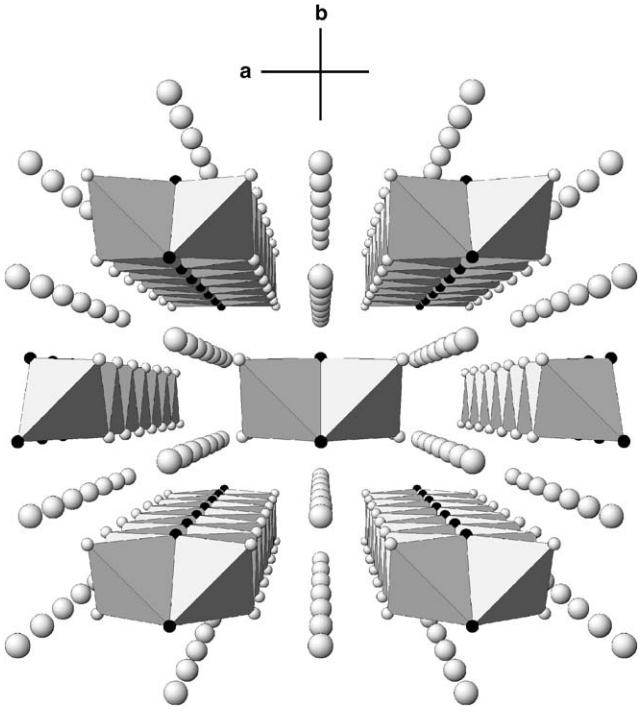

Fig. 2. Perspective view of the structure of the $A Fe_2S_3$ alkali thioferrates (A = Cs, Rb, K, Ba) down the c-axis. Pairs of edge-sharing FeS_4 polyhedra form double chains extending along [001]. Alkali elements (spheres) occur in 10-fold coordination with S between these double chains.

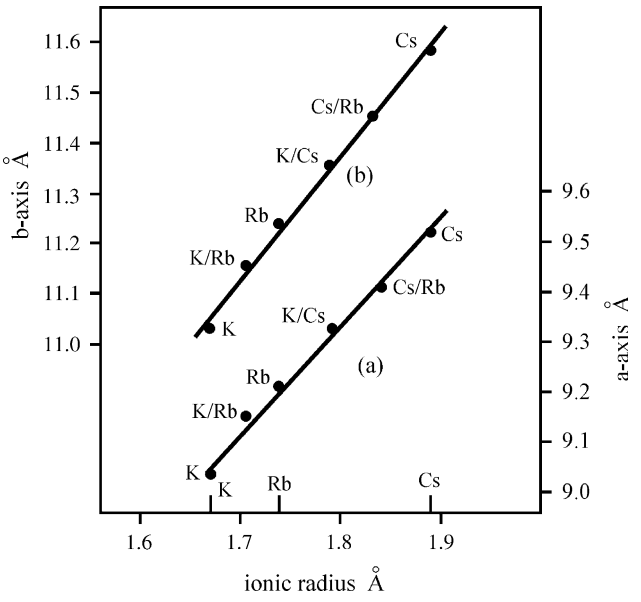

Fig. 3. Relationships between the a and c dimensions of alkali thioferrates and the ionic radius of the inter-chain cation in 10-fold coordination. For intermediate compounds the average ionic radius of the A-site atoms is used, i.e. $(x \cdot r_i + y \cdot r_j)$; where x and y are the weight fractions of A-site cations i and j, in the solid solution.

Table 4
Selected bond lengths (Å), polyhedral volumes, distortion parameters, and bond valence sums of $A Fe_2S_3$ rasvumites (A = Cs, Rb, K)

	$CsFe_2S_3$	$RbFe_2S_3$	KFe_2S_3
A–S(1)	3.712(1) × 2	3.629(1) × 2	3.562(1) × 2
A–S(2)	3.581(1) × 4	3.472(1) × 4	3.401(1) × 4
A–S(2)	3.657(1) × 2	3.541(1) × 2	3.468(1 × 2
A–S(2)	3.868(1) × 2	3.775(1) × 2	3.738(1) × 2
Mean	3.680	3.578	3.514
δ	0.837	1.020	1.299
Δ(Å^3)	101.53	93.42	88.68
A-shift	0.099	0.087	0.027
BV_{10}	1.226	0.974	0.868
Fe–S(1)	2.343(1) × 2	2.335(1) × 2	2.310(1) × 2
Fe–S(2)	2.213(1) × 2	2.208(1) × 2	2.212(1) × 2
Mean	2.278	2.272	2.259
δ	0.819	0.771	0.439
Δ (Å^3)	6.04	6.00	5.910
Fe-shift	0.065	0.083	0.081
BV_4	2.954	3.002	3.072
HSV	2.618	2.666	2.770
Fe–Fe(c)	2.741	2.723	2.709
Fe–Fe(a)	2.699	2.716	2.734
τ	108.89°	110.43°	110.54°

δ = polyhedron distortion parameter [19]; Δ = polyhedron volume; BV = bond valence sum calculated by IVTON (Balić-Zunić and Vicković [20]; HSV = calculated [15] empirical valence of Fe; τ = tetrahedral thickening angle, ideally 109.47° for a distortion-free tetrahedron.

Table 1 and Fig. 3 show that, as expected, cell dimensions and volumes increase linearly as the size of the alkali cation increases. Table 4 lists selected bond lengths and polyhedron volumes and shows that the expansion of the lattice is related entirely to the increase in size of the AS_{10} polyhedron from 88.7 Å^3 in KS_{10} to 101.5 Å^3 in CsS_{10}, as the size of the FeS_4 polyhedra are similar throughout the entire series. As the size of AS_{10} increases the displacement of the A-cation from the center of the polyhedron along the b-axis increases, i.e., from 0.3 Å in KS_{10} to 1.1 Å in CsS_{10}. Accompanying this displacement there is actually a slight decrease in the amount of distortion of the AS_{10} polyhedron and a change in the bond valence character, as determined from the bond valence sum [11] of S about the A-cation, from slightly underbonded to overbonded relative to an ideal value of +1.

In contrast to the AS_{10} polyhedra, FeS_4 tetrahedra comprising the chains exhibit an increase in distortion (Table 4) with increasing size of the alkali cation in the structure, coupled with a slight change in the bonding character, as determined from the bond valence sum [11] of S about Fe, from overbonded to underbonded (Table 4) relative to an ideal value of +3.0. The displacement of the Fe atoms along the a-axis from the centers of the FeS_4 polyhedra decreases slightly from 0.7 Å in KFe_2S_3 to 0.62 Å in $CsFe_2S_3$. These changes are associated with varying Fe–Fe distances in the edge-sharing tetrahedra which increase along c and decrease along a (Table 4). Distortion parameters and cation displacements of the

Table 5
Selected bond lengths (Å), polyhedral volumes and distortion parameters for solid solutions of AFe_2S_3 rasvumites (A = Cs, Rb, K)

	$(Cs_{0.5}Rb_{0.5})Fe_2S_3$	$(Cs_{0.5}K_{0.5})Fe_2S_3$	$(K_{0.5}Rb_{0.5})Fe_2S_3$
A–S(1)	3.671(1) × 2	3.654(1) × 2	3.632(1) × 2
A–S(2)	3.510(1) × 4	3.498(1) × 4	3.447(1) × 4
A–S(2)	3.640(1) × 2	3.571(1) × 2	3.525(1) × 2
A–S(2)	3.820(1) × 2	3.826(1) × 2	3.738(1) × 2
Mean	3.630	3.610	3.559
δ	1.011	1.159	1.045
Δ (Å^3)	97.74	95.79	91.98
A-shift	0.102	0.099	0.085
Fe–S(1)	2.358(1) × 2	2.368(1) × 2	2.308(1) × 2
Fe–S(2)	2.247(1) × 2	2.217(1) × 2	2.208(1) × 2
Mean	2.303	2.293	2.258
δ	0.573	1.077	0.490
Δ (Å^3)	6.253	6.160	5.887
Fe-shift	0.051	0.105	0.078
Fe–Fe(c)	2.735	2.730	2.719
Fe–Fe(a)	2.706	2.774	2.711

δ = polyhedron distortion parameter [19]; Δ = polyhedron volume.

binary solid solutions (Table 5) follow the trends noted for the end-member compositions.

4. Oxidation state of iron

The synthesized mixed valence thioferrates are isostructural with *Cmcm* rasvumite [1], $BaFe_2S_3$ [12], $RbFe_2Se_3$, $RbFe_2Te_3$, $CsFe_2Se_3$, $CsFe_2Te_3$ [4], and $CsCu_2Cl_3$ [13]. The compound $BaFe_2Se_3$ adopts space group *Pnma* and has a similar but slightly distorted structure [12]. These alkali element chalcogenides are interesting with respect to the mixed valence state of iron. This arises because the compounds are not entirely ionic. Whereas the bonds between the alkali cations and sulfur are predominantly ionic, those between Fe and S in the FeS_4 tetrahedra are predominantly covalent. Accordingly, electrons are delocalized and Fe cannot be assigned a single valence state. The electron delocalization is expressed conventionally in studies of alkali thioferrates as an calculated empirical non-integral valence [1,14,15].

In $BaFe_2S_3$ iron is predicted, assuming the compound is ionic, to be entirely as Fe^{2+}, whereas in "ionic" KFe_2S_3, iron should have an oxidation state intermediate between Fe^{3+} and Fe^{2+}, i.e., $Fe^{2.5+}$. As there is only one crystallographic site for Fe in these alkali thioferrates there cannot be an ordered distribution of Fe^{2+} and Fe^{3+} to arrive at this average valence. Mössbauer studies of $BaFe_2S_3$ [14] indicate that iron is present in the non-integral empirical oxidation state of $Fe^{2.5+}$ rather than as Fe^{2+}. This observation is supported by the oxidation state of +2.64 calculated using the semi-empirical relationship between Fe–S bond distances and oxidation state proposed by Hoggins and Steinfink [15]. Mössbauer data for KFe_2S_3 [16] indicate the empirical oxidation state of iron is +2.75 rather than +2.5. Klepp et al. [4] note that an increase in the formal oxidation state of iron also affects the Fe–Fe distances along the chains of tetrahedra. In the compounds prepared in this study this parameter increases from 2.709 Å in KFe_2S_3 to 2.741 Å in $CsFe_2S_3$, corresponding to a change in the calculated valency [15] of Fe from +2.77 to +2.62 (Table 4). Similar relationships are found for the Ba-, Rb-, and Cs- selenoferrates [4]. Goodenough et al. [17] have suggested that the observed increases in Fe–Fe distances are related to delocalization of the electrons of Fe^{2+} along the chain directions, with the remaining electrons localized between the two iron atoms orthogonal to the chain. Our data for all the alkali thioferrates appear to support this conclusion. However, our data, and those of Klepp et al. [4], clearly indicate that the character of the inter-chain atoms must also control the observed empirical oxidation state of iron. This implies that interactions between the strongly electropositive alkali element cations occupying the AS_{10} polyhedra and the FeS_4 tetrahedra must also occur. Increase in size of the AS_{10} polyhedra leads to a weaker A–S ionic bond. For example the Coulombic pair potential bond strength, a measure of ionic bond strength [18], for the Cs–S bond is only 95.5% of that of the K–S bond. This slightly weaker bond might result in a higher degree of overlap between Fe and S orbitals in the chains and increased Fe–Fe repulsion. From previous studies it is apparent that alkali chalcogenides exhibit metallic conductivity and are strongly anisotropic with respect to their electrical resistivity [15]. However, the character of the bonding between Fe and S within the tetrahedra is not well-established. Studies of separate and interconnected edge-sharing FeS_4 tetrahedra in Na_5FeS_4 and $KFeS_2$, respectively, indicate that iron is present as high spin Fe^{3+} [17,19]. As the FeS_4 polyhedra in the single chains of tetrahedra in $KFeS_2$ are very similar (Fe–Fe = 2.706 Å; Fe–S = 2.196 and 2.280 Å) to those in KFe_2S_3, it is suggested that all of the iron in the mixed valence ferrites is present in a high spin state. However, resolution of the exact electronic configuration of Fe in the FeS_4 chains of these alkali thioferrates requires detailed studies of X-ray absorption and Mössbauer spectra coupled with measurements of the magnetic susceptibility.

5. Conclusions

The structures of the $CsFe_2S_3$ and $RbFe_2S_3$ are isomorphous with that of KFe_2S_3. Binary solid solutions between these end-member compositions adopt the same structure and also crystallize in space group *Cmcm*

(#63), implying that there is a continuous solid solution in the ternary system $CsFe_2S_3$–$RbFe_2S_3$–KFe_2S_3. These mixed valence alkali thioferrates show regular changes in cell dimensions, AS_{10} polyhedron volumes, polyhedra distortion parameters, and the empirical oxidation state of Fe with respect to increasing size of the alkali element cation. Further investigations of their magnetic and electrical properties are required to determine their electronic structure and bonding character.

References

[1] J.R. Clark, G.E. Brown, Am. Mineral. 65 (1980) 477–482.
[2] M.N. Sokolova, M.G. Dobrovolskaya, N.I. Organova, M.E. Kazkova, A.L. Dmitrik, Zap. Vses. Mineral. Obshch. 99 (1970) 712–720.
[3] A.R. Chakhmouradian, R.H. Mitchell, L. Horvath, GAC-MAC Ann. Mtg. Abstracts with Program St. Johns 26 (2001) 24.
[4] K.O. Klepp, W. Sparlink, H. Boller, J. Alloys Compd. 238 (1996) 1–5.
[5] G. Brauer, Handbook of Preparative Inorganic Chemistry, Vol. 2, Academic Press, New York.
[6] A.A. Kern, A.A. Coelho, TOPAS 2.1, 1998, www.bruker-axs.com.
[7] J.J. Rodriguez-Carvajal, FULLPROF 2000, www.llb.cea.fr/full-web/powder.htm
[8] W. Bronger, A. Kyas, P. Muller, J. Solid State Chem. 70 (1987) 262–270.
[9] W. Bronger, Z. Anorg. Allg. Chem 359 (1968) 225–233.
[10] E.J. Fasiska, Phys. Stat. Solidi 10A (1972) 165–173.
[11] I.D. Brown, Acta Crystallogr. B 48 (1992) 553–572.
[12] H.Y. Hong, H. Steinfink, J. Solid State Chem. 5 (1972) 93–104;
C. Brink, N.F. Binnendijk, J. Van de Linde, Acta Crystallogr. 7 (1954) 176–180.
[13] W.M. Reiff, I.E. Grey, A. Fan, Z. Eliezer, H. Steinfink, J. Solid State Chem. 13 (1975) 32–40.
[14] J.T. Hoggins, H. Steinfink, Inorg. Chem. 15 (1976) 1682–1685.
[15] G. Amthauer, K. Bente, Naturwissenschaften 70 (1983) 146–147.
[16] J.B. Goodenough, Mater. Res. Bull. 13 (1978) 1305–1308.
[17] G.S. Rohrer, Structure and Bonding in Crystalline Materials, Cambridge University Press, Cambridge, 2001.
[18] M. Atanasov, R.H. Potze, G.A. Sawatzky, J. Solid State Chem. 119 (1995) 380–393.
[19] R.D. Shannon, Acta Crystallogr. A 32 (1976) 751–767.
[20] T. Balić-Žunić, I.J. Vicković, J. Appl. Crystallogr. 29 (1996) 305–306.